

# Solar internal sound speed as inferred from combined BiSON and LOWL oscillation frequencies

Sarbani Basu,<sup>1</sup> W. J. Chaplin,<sup>2</sup> J. Christensen-Dalsgaard,<sup>1</sup> Y. Elsworth,<sup>2</sup> G. R. Isaak,<sup>2</sup> R. New,<sup>3</sup> J. Schou,<sup>4</sup> M. J. Thompson<sup>5</sup> and S. Tomczyk<sup>6</sup>

<sup>1</sup>*Teoretisk Astrofysik Center, Danmarks Grundforskningsfond, Institut for Fysik og Astronomi, Aarhus Universitet, DK-8000 Aarhus C, Denmark*

<sup>2</sup>*School of Physics and Space Research, University of Birmingham, Edgbaston, Birmingham, B15, 2TT, U.K.*

<sup>3</sup>*School of Science and Mathematics, Sheffield Hallam University, Sheffield, S1 1WB, U.K.*

<sup>4</sup>*Center for Space Science and Astrophysics, HEPL Annex A201, Stanford University, Stanford, CA 94305, U.S.A*

<sup>5</sup>*Astronomy Unit, School of Mathematical Sciences, Queen Mary and Westfield College, London E1 4NS, U.K.*

<sup>6</sup>*High Altitude Observatory, NCAR, P.O. Box 3000, Boulder, CO 80307, U.S.A.*

Accepted . Received

## ABSTRACT

Observations of the Sun with the LOWL instrument provide a homogeneous set of solar p-mode frequencies from low to intermediate degree which allows one to determine the structure of much of the solar interior avoiding systematic errors that are introduced when different data sets are combined, i.e., principally the effects of solar cycle changes on the frequencies. Unfortunately, the LOWL data set contains very few of the lowest-degree modes, which are essential for determining reliably the structure of the solar core – in addition, these lowest-degree data have fairly large associated uncertainties. However, observations made by the Birmingham Solar-Oscillations Network (BiSON) in integrated sunlight provide high-accuracy measurements of a large number of low-degree modes. In this paper we demonstrate that the low-degree mode set of the LOWL data can be successfully combined with the more accurate BiSON data, provided the observations are contemporaneous for those frequencies where the solar-cycle-induced effects are important. We show that this leads to a factor-of-two decrease in the error on the inferred sound speed in the solar core. We find that the solar sound speed is higher than in solar models for  $r < 0.2R_{\odot}$ . The density of the solar core is, however, lower than that in solar models.

**Key words:** methods: data analysis — Sun: interior — Sun: oscillations

## 1 INTRODUCTION

Observations of the Sun, covering many years, have now provided us with accurate measurements of solar p-mode frequencies which impose severe constraints on the structure of the Sun.

The LOWL instrument (LOWL is an abbreviation for low degree with degree denoted by L) has, for the first time, provided us with a uniform set of frequencies from low to intermediate degree  $l$ . This has allowed detailed inversions for the structure of much of the Sun’s interior (cf., Basu et al. 1995; 1996a; 1996b) to be performed. The available data from the instrument now span a period of more than 1 year, and most of the mode-frequency determinations have relative errors as small as a few parts in  $10^6$ .

The LOWL data set contains very few of the lowest-degree modes, i.e., for  $0 \leq l \leq 2$ , and those that are present have much larger errors than their higher- $l$  counterparts. Since only the low-degree modes penetrate to the solar core,

large uncertainties in the inferred structure of the solar core arise from inversions which rely solely on these data. Observations made by the Birmingham Solar-Oscillations Network (BiSON) do, however, provide very accurate measurements of low-degree modes (cf. Elsworth et al. 1994). These modes have to be combined with intermediate and high-degree modes from other sources before they can be used to infer the solar structure by inverting the observed frequencies – it would therefore seem logical to combine the BiSON and LOWL solar data in order to provide a more reliable determination of the structure of the solar core.

Great care must be taken in combining data from different sources. Systematic differences may arise from differences in instrument characteristics and analysis techniques, or from temporal variations in the solar p-modes if the different observations are not contemporaneous. Such differences may be interpreted by an inversion as being solar in origin, and in particular in the present context as arising from *spatial* variations in the solar interior.

**Table 1.** Summary of data sets

	Name	Summary details
1	BiSON-8	8-month BiSON spectrum; maximum likelihood analysis
2	BiSON-G	Five 2-month BiSON spectra, Gaussian-analysed
3		Lower frequency data from 32-month BiSON spectrum; maximum likelihood analysis
4		Comparison BiSON data taken at high solar activity; Gaussian-analysed
5	LOWL	1-year spatially-resolved LOWL data
6	Best Set	Combination of BiSON sets 1-3 and LOWL

The issue of combining non-contemporaneous data is particularly important, because it is known that the p-mode frequencies change along the solar cycle (Libbrecht & Woodard 1990; Elsworth et al. 1994). The difficulties in determining the solar core structure from inhomogeneous data sets have been discussed by Gough & Kosovichev (1993), Gough, Kosovichev & Toutain (1995) and Basu et al. (1995, 1996a). The solar-cycle variations are believed to be the result primarily of variations in the surface properties of the Sun. It may therefore be possible that the temporal variations can be removed in the inversion in the same way as other surface uncertainties (cf. Dziembowski et al. 1991; Kosovichev et al. 1992) but, as was pointed out by Basu et al. (1996a), there remain significant problems in the combination procedure and the resulting inversions may be misleading.

We have largely avoided such problems in the present work by combining near-contemporaneous data from the BiSON network and the LOWL instrument, taken at a low-activity phase of the solar cycle. We also use some low-frequency BiSON data based on observations over several years, but such low-frequency modes will be relatively insensitive to solar-cycle variations in the near-surface layers (cf. Libbrecht & Woodard 1990). We also present results of combining LOWL with BiSON data collected at times of high solar activity, to illustrate the dangers inherent in inverting non-contemporaneous data.

## 2 THE DATA

The data used for the analysis come from two sources: the LOWL instrument based on Mauna Loa (Tomczyk et al. 1995) in the Hawaiian Islands; and the global, 6-station BiSON network (Chaplin et al. 1996a). Both systems employ the same basic physical principles – the use of an atomic standard – to measure the Doppler velocity shift of a solar Fraunhofer line formed by potassium atoms in the near infrared (770 nm). The LOWL instrument spatially resolves the visible solar disc, and is therefore sensitive to oscillation modes of degree up to  $l = 99$ . The BiSON instruments view the unresolved Sun, and are sensitive to modes of  $0 \leq l \leq 4$ . Although limited to the lowest- $l$  modes, the BiSON technique is very stable and provides some of the highest-quality measures of those modes available. The combination of these two data sets should be very powerful given that: they result from observations made on the same line in the solar atmosphere; each are characterized by high intrinsic accuracies;

and both were collected at the same epoch.

The LOWL time series used for the analysis covers a 12 month period beginning 1994 February 26 and has a temporal duty cycle of 22 per cent. Further details of the LOWL experiment are given by Tomczyk et al. (1995). The data were analysed up to 3.5 mHz, which thus set the upper limit to the frequency range used in this paper, while the lower limit was set by the visibility of the modes in the data set. The fitting procedure, which is a maximum-likelihood technique applied to the complex Fourier transform of the time series, is described in Appendix 5 of Schou (1992).

Several BiSON data sets have been used: these are summarised briefly in Table 1. For reasons of convenience, we have used an 8-month BiSON spectrum within the time span of the LOWL set (henceforth referred to as BiSON-8), generated from data collected between 1994 January 26 and 1994 September 22. The duty cycle of the BiSON-8 time series was 80 per cent. The modes in the Fourier spectra generated from the BiSON-8 time series were fitted by minimizing a maximum-likelihood function that assumed an underlying  $\chi^2$  distribution with two degrees of freedom in the frequency domain (e.g., Anderson, Duvall & Jefferies 1990; Toutain & Appourchaux 1994).

In addition, we have fitted frequencies from five 2-month BiSON spectra (which are contemporaneous with the LOWL data). The duty cycle for the complete calendar year 1994 was 78 per cent. The modes in the 2-month BiSON spectra were first smoothed before fitting to yield pseudo-Gaussian statistics in the frequency domain – these data are therefore referred to as the BiSON-G set.

To get reliable determinations of the lowest-degree modes at frequencies below 1.8 mHz one requires spectra generated from more than 1 year’s data, and for this reason we used results derived from the not-entirely contemporaneous 32-month BiSON spectrum. These modes are not expected to be influenced significantly by the solar cycle, and we do in fact demonstrate that their inclusion in the analysis does not bias the results. Mode frequencies were obtained from a single, 32-month BiSON spectrum of observations between 1992 October and 1995 June (Chaplin et al. 1996b). The fractional fill of useful data was 72 per cent. The spectrum was analysed in the same way as the 8-month spectrum.

Finally, to show that variations in p-mode frequencies over the solar-cycle do have a deleterious effect on structural inversions, we have used a set of frequencies derived from BiSON observations made at times of high solar activity. These data are described by Elsworth et al. (1994).

The fitted BiSON frequencies at  $l = 0$  and 1 were, in general, more accurate than their LOWL counterparts; for  $l = 2$ , the quality of the data were similar; while for  $l = 3$ , the LOWL frequencies were, by and large, better determined. We have derived a “Best Set” of frequencies by merging the available data, giving due and careful consideration to the comparative quality of the frequency determinations in each set (see later). The LOWL and BiSON data sets are plotted in Fig. 1 in the form of an  $l$ - $\nu$  diagram. Because the lower turning points of the modes in the combined data set span the range of most radii from the Sun’s surface to its centre, and because the errors on the frequencies are very small, it is feasible to perform a meaningful inversion for the solar structure throughout most of the interior.

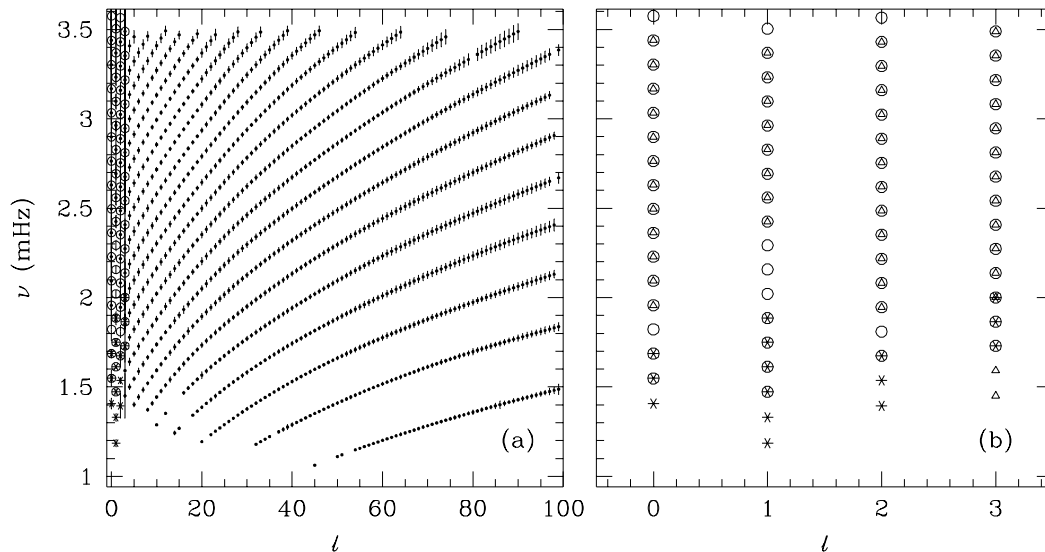


**Figure 1.** The  $l$ - $\nu$  diagram of the data used. Panel (a) shows the entire range with  $1000\sigma$  error bars, while panel (b) shows just the low-degree modes. The triangles (dots in panel a) are LOWL modes; circles are BiSON-8 modes; asterisks are 32-month BiSON modes.

### 3 INVERSION TECHNIQUES AND SOLAR MODELS

Solar oscillations can be described throughout most of the solar interior by equations describing linear adiabatic oscillations (cf. Unno et al. 1989). Chandrasekhar (1964) showed that these equations, along with appropriate boundary conditions, constitute a self-adjoint eigenvalue problem, which leads to a variational principle connecting the eigenfrequencies to the basic equilibrium state of the Sun.

Our inversion for solar structure is based on linearizing the equations of stellar oscillation around a known reference model (cf., Dziembowski, Pamyatnykh & Sienkiewicz 1990; Däppen et al. 1991; Antia & Basu 1994; Dziembowski et al. 1994). The differences between the structure of the Sun and the reference model are then related to the differences in the frequencies of the Sun and the model by kernels.

Non-adiabatic effects give rise to frequency shifts (Cox & Kidman 1984; Balmforth 1992) which are not accounted for by the variational principle. Frequency shifts are also introduced by errors in modelling the underlying solar model, e.g., the effects of turbulent convection. Most of these uncertainties affect the surface layers of the models. In the absence of any reliable formulation, these effects have been taken into account in an *ad hoc* manner by including an arbitrary function of frequency in the variational formulation (Dziembowski et al. 1990). This can be justified because in the surface layers, the eigenfunction is largely independent of the degree  $l$  of the mode; thus, for spherically symmetric perturbations, the frequency difference resulting from the surface effects, weighted by the inertia of the mode, is roughly a function of frequency only (Christensen-Dalsgaard & Berthomieu 1991). We thus express the fractional change in frequency of a mode in terms of fractional changes in the model parameters and also a surface effect.

When the oscillation equation is linearised – under the assumption of hydrostatic equilibrium – the fractional change in the frequency can be related to the fractional

changes in two of the model parameters. Thus,

$$\frac{\delta\omega_i}{\omega_i} = \int K_{1,2}^i(r) \frac{\delta f_1(r)}{f_1(r)} dr + \int K_{2,1}^i(r) \frac{\delta f_2(r)}{f_2(r)} dr + \frac{F_{\text{surf}}(\omega_i)}{Q_i} \quad (1)$$

(cf. Dziembowski et al. 1990). Here  $\delta\omega_i$  is the difference in the frequency  $\omega_i$  of the  $i$ th mode between the solar data and a reference model. The functions  $f_1$  and  $f_2$  are an appropriate pair of model parameters. The kernels  $K_{1,2}^i$  and  $K_{2,1}^i$  are known functions of the reference model which relate the changes in frequency to the changes in  $f_1$  and  $f_2$  respectively; and  $Q_i$  is essentially the inertia of the mode (Christensen-Dalsgaard 1986). The term in  $F_{\text{surf}}$  results from the near-surface errors.

The pair of variables  $(f_1, f_2)$  can involve several combinations of model parameters. As discussed below, our goal in the inversion is to isolate one of the variables while endeavouring to ensure that our results are insensitive to the other variable. In this work we generally use  $(c^2, \rho)$ ,  $c$  being adiabatic sound speed and  $\rho$  density, to invert for  $c^2$ . To invert for density, one good pair to use is  $(\rho, \Gamma_1)$ , where  $\Gamma_1$  is the first adiabatic exponent. Alternatively, one may assume the equation of state to be known and transform the dependence of the oscillations on  $\Gamma_1$  into a dependence instead on  $Y$  ( $Y$  being the abundance by mass of helium), to carry out inversion for the pair  $(\rho, Y)$ . (As formulated, this also assumes that the heavy element abundances are known.) We have used this formulation, which has the advantage that the frequency dependence on  $Y$  is largely confined to the helium ionization zones. This is easier to suppress in the inversion for density than the dependence on  $\Gamma_1$  would be in an inversion using  $(\rho, \Gamma_1)$ . Consequently we can achieve better resolution and/or error properties in our density inversion. However, this advantage is bought by assuming the equation of state to be known, a point to which we return in Section 5.

A number of different inversion techniques can be used for inverting the constraints given in equation (1). We have used the subtractive optimally localised averages (SOLA) method of Pijpers & Thompson (1992).

The principle of the inversion technique is to form linear combinations of equations (1) with weights  $c_i(r_0)$  chosen such as to obtain an average of  $\delta f_1/f_1$  localized near  $r = r_0$  while suppressing the contributions from  $\delta f_2/f_2$  and the near-surface errors. In addition, the statistical errors in the combination must be constrained. If successful, the result may be expressed as

$$\int \mathcal{K}(r_0, r) \frac{\delta f_1(r)}{f_1(r)} dr \simeq \sum c_i(r_0) \frac{\delta \omega_i}{\omega_i}, \quad (2)$$

where the  $\mathcal{K}(r_0, r)$ , the averaging kernel at  $r = r_0$ , is defined as

$$\mathcal{K}(r_0, r) = \sum c_i(r_0) K_{1,2}^i(r), \quad (3)$$

of unit integral, and determines the extent to which we have achieved a localized measure of  $\delta f_1/f_1$ . In particular, the width in  $r$  of  $\mathcal{K}(r_0, r)$ , here calculated as the distance between the first and third quartile point, provides a measure of the resolution<sup>†</sup>. The precise implementation of the method is described by Basu et al. (1995, 1996c).

A drawback of the SOLA method is the implicit assumption that the frequency differences and the errors associated with them are correct. However, sometimes the observational errors can be either under- or overestimated (e.g. because the modes have much lower line widths than modes adjacent in frequency), in which case the inversion result can be misleading. We have found that a reliable way to detect such modes is to do a regularized least squares (RLS) inversion first. We rejected modes which had more than a  $3.5\sigma$  residual after the fit. The SOLA inversion was performed on the weeded mode set. On examining some of the low-degree modes that had been rejected by the RLS procedure, we found that the fit to the mode concerned was usually poor. Thus the RLS is a reasonably reliable way of weeding out uncertain modes. There are some interesting instances where, even in contemporaneous data, the appearance of a particular mode was very different in each data set, presumably because of beating with noise. In addition, different analysis techniques can give rise to fitted frequencies which differ by more than the formal error. The details of the RLS implementation can be found in Antia & Basu (1994).

Our inversion requires the use of a reference solar model. The model we use (Model S of Christensen-Dalsgaard et al. 1996) was constructed with the Livermore (OPAL) equation of state (Rogers, Swenson & Iglesias, 1996). For temperatures higher than  $10^4$  K, OPAL opacities are used (Iglesias, Rogers & Wilson 1992), whereas at lower temperatures opacities from the tables of Kurucz (1991) are taken. The model incorporates the diffusion of helium and heavy elements below the convection zone. The surface heavy element ratio is  $Z/X = 0.0245$  (Grevesse & Noels 1993). The model has an

<sup>†</sup> The radii  $r_1, r_2, r_3$  of the first, second and third quartile points are defined such that  $\mathcal{J}(r_1) = 0.25$ ,  $\mathcal{J}(r_2) = 0.5$  and  $\mathcal{J}(r_3) = 0.75$ , where  $\mathcal{J}(r) = \int_0^r \mathcal{K} dr$  (recall that  $\mathcal{K}$  is unimodular). In practice this uniquely defines  $r_1, r_2$  and  $r_3$  for our kernels.

**Table 2.** Properties of solar models

Model	$(Z/X)_s$	$Y_e$	$Y_c$	$T_c$ 10 <sup>6</sup> K	$\rho_c$ g cm <sup>-3</sup>	$r_d/R_\odot$	Age Gyr
Reference	0.0245	0.2447	0.6444	15.67	154.2	0.7115	4.6
Test	0.0245	0.2457	0.6402	15.64	152.9	0.7124	4.52

Notes:  $(Z/X)_s$  is the present surface heavy element abundance ratio;  $Y_e$  and  $Y_c$  are the current envelope and central helium abundances respectively;  $T_c$  is the central temperature,  $\rho_c$  the central density, and  $r_d/R_\odot$  the radial location of the base of the convective envelope in the models used in this paper.

age of 4.6 Gyr. We have also used another model as a proxy Sun to illustrate certain effects. The physical assumptions in the model are identical to those in the reference model, but it has a lower age of 4.52 Gyr. Some of the properties of the models are listed in Table 2.

## 4 RESULTS

### 4.1 Consistency of the frequencies

To illustrate the effects of the solar cycle on the observed frequencies, the frequency differences between the LOWL and the BiSON-8 and BiSON high-activity data have been plotted in Fig. 2. The high-activity BiSON data show a systematic, frequency-dependent difference with respect to the LOWL data. The BiSON-8 data show no such trend. Since slowly varying, frequency-dependent terms in the differences are caused by perturbations near the solar surface (e.g. Gough 1990), this implies that while the BiSON-8 and LOWL data show similar surface effects, the BiSON high-activity data do not. The differences between the high-activity BiSON and LOWL data are indicative of the influence of the solar cycle. Consequently, if the low-degree LOWL data were to be replaced by the high-activity BiSON data, the combined mode set would have two different surface terms.

This effect is seen quite clearly in Fig. 3(a), which shows differences between the LOWL, BiSON-8 and BiSON high-activity data and frequencies of the reference solar model. The frequency differences have been weighted with the corresponding mode inertia in order to compensate for the fact that, for given a discrepancy in the model or mode physics, deeply penetrating modes are perturbed less than modes which have a shallow turning point (cf. Christensen-Dalsgaard & Berthomieu 1991). To show the general trend of the LOWL data, we have also plotted the frequency differences of higher-degree modes. While the BiSON-8, LOWL, and 32-month BiSON data follow the same trend, the high-activity BiSON data lie above this.

Owing to the manner in which the inversion techniques are implemented, they would be unable to isolate the two separate frequency dependent trends resulting from the combination of the high- and low-activity data. This would, of course, give rise to misleading inversion results (cf. Basu et al. 1995, 1996a). The BiSON-8 and LOWL data show no systematic differences, however, and we should therefore be able to combine these two data sets.

Asymptotically, the frequency differences can be written as (e.g. Christensen-Dalsgaard, Gough & Pérez Hernández 1988)

$$S(w)\delta\omega/\omega = H_1(w) + H_2(w), \quad (4)$$

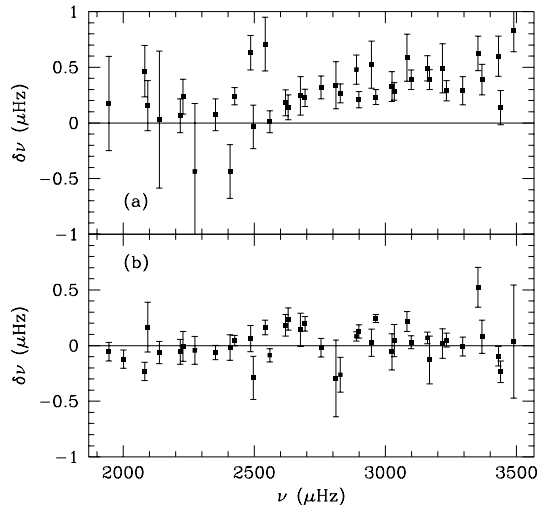


**Figure 2.** (a) The frequency differences between the high-activity BiSON and LOWL data sets. (b) The frequency differences between the BiSON-8 and LOWL data sets. The error bars on each plot were generated by adding the respective BiSON and LOWL uncertainties in quadrature.

where  $w = \omega/(l + 0.5)$ , and  $S(w)$  is a known function of the reference model. The function  $H_1(w)$  depends on the sound-speed difference between the Sun and the reference model and  $H_2(\omega)$  is determined by differences at the surface. In Fig. 3(b) we have plotted the residuals after the functions  $H_1$  and  $H_2$  – each obtained by fitting the LOWL data – have been removed from the frequency differences. Note that the residuals for the high-activity BiSON data are much larger compared with those for the other sets, and follow a completely different trend.

#### 4.2 Consistency of inversion results

Once the consistency of the different data sets had been established, we proceeded to invert for the sound-speed difference between the Sun and the reference model, comparing results of different combinations of LOWL and BiSON data. The results of the inversions are shown in Fig. 4. To provide a common reference, all panels include the results of inverting the LOWL data only.

First, in Fig. 4(a) we replaced the  $l = 0, 1,$  and  $2$  modes of the LOWL set with those of BiSON-8 or high-activity BiSON data. Only those modes which were common in all sets were used – this ensured that the resultant resolution of the inversions would be comparable. Since the mode sets used for the inversions were identical for  $l > 2$ , any differences in the results should be confined to the core region – this is indeed found to be the case. As anticipated, the results of the inversion which utilized the high-activity BiSON set were markedly different from those based on data from the same epoch. This effect was first noted by Basu et al. (1996a), and is a result of the different surface effects in the high and low-activity data. As can be seen in the figure, the inversion results from the LOWL set and the LOWL plus BiSON-8 set are fairly consistent – the contemporaneous BiSON-8 and LOWL sets can therefore be satisfactorily combined. Similarly, inversion results [Fig. 4(b)] generated by substituting the low-degree data from the BiSON-G set show no basic

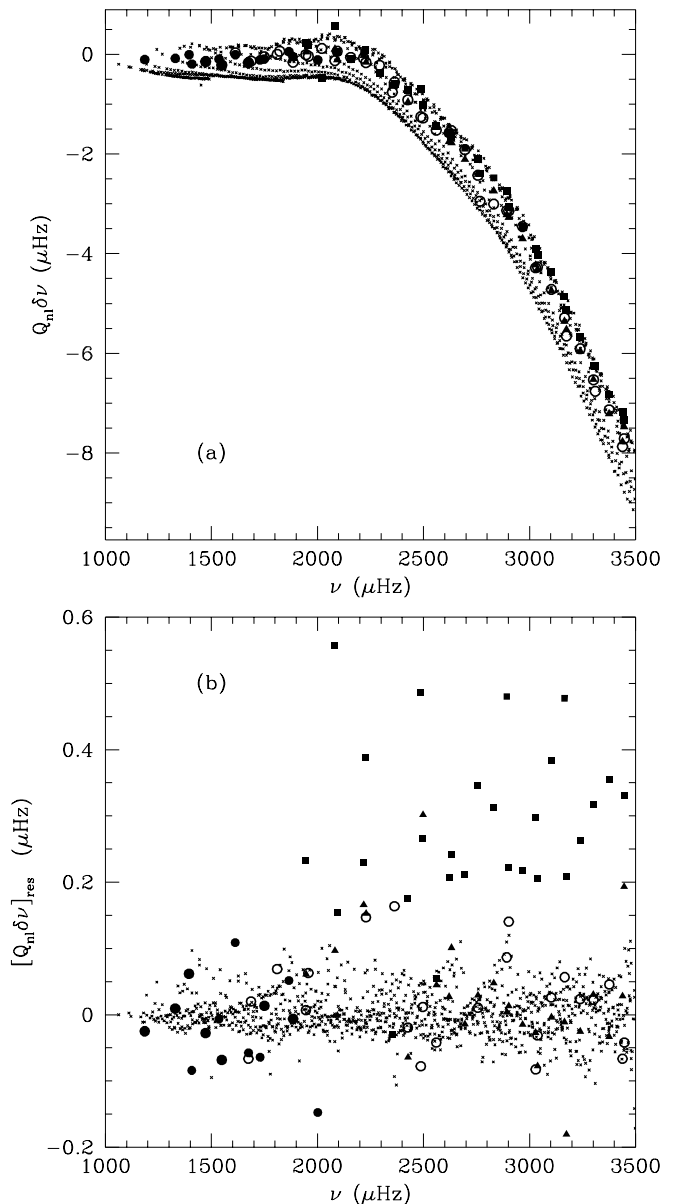


**Figure 3.** (a) The frequency difference between the different data sets and the reference model, in the sense (Sun) – (Model), scaled by the mode inertia  $Q_{nl}$ , which is essentially the function  $S$  (cf. eq. 4) normalised by the acoustic radius of the star. (b) The residuals after the function  $H_1(w) + H_2(\omega)$  has been removed from the scaled frequency differences. The tiny crosses are LOWL data for degrees 3 to 10; the filled triangles are LOWL data for degrees 0–2; the empty circles are BiSON-8 data; the filled circles are the 32-month BiSON data; and the filled squares are BiSON data obtained at high solar activity.

inconsistency; thus, although fitted by a different technique, these mode frequencies can be used in a combined data set.

As a final step, we supplemented the input data with those low-degree modes – from the BiSON-8 and 32-month BiSON sets – not present in the LOWL set. The results are shown in Fig. 4(c). Adding the extra modes does not change the general trend of the result, although there are noticeable improvements in resolution and errors.

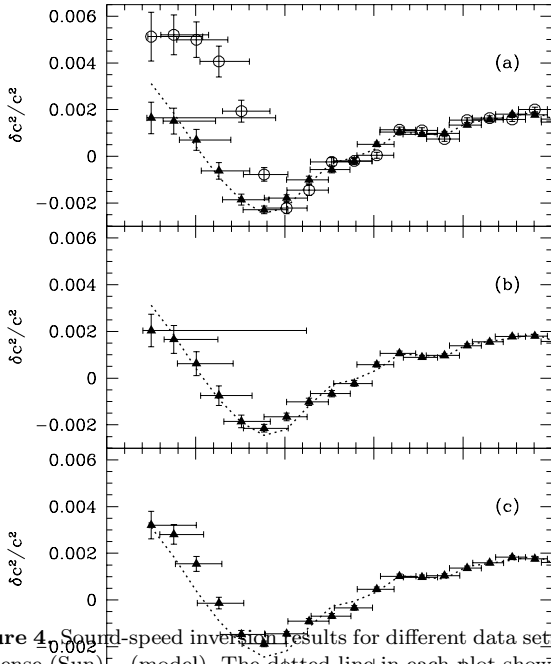


**Figure 4.** Sound-speed inversion results for different data sets, in the sense (Sun) - (model). The dotted line in each plot shows the results from an inversion performed on the LOWL data only, while the symbols are for different combinations of LOWL and BiSON data. The vertical  $1\text{-}\sigma$  error bars show the propagated data errors and the horizontal bars extend from the first to the third quartile point of the averaging kernels, to indicate the resolution of the inversion. (a) The triangles were obtained by using BiSON-8 data for those modes with  $0 \leq l \leq 2$  which are common to the LOWL and BiSON-8 sets; the circles show the results of substituting the high-activity BiSON data in a similar fashion. (b) The triangles show the results from a set where LOWL data for  $0 \leq l \leq 2$  have been replaced by BiSON-G data. (c) The triangles show the results from a set where LOWL data for  $0 \leq l \leq 2$  have been replaced by BiSON-8 data; additional mode frequencies from the BiSON-8 and 32-month BiSON sets – not available in the LOWL set – have also been introduced.

### 4.3 The “best” mode set

Having ascertained that the BiSON and LOWL data sets were compatible, we selected a “best” low-degree mode set for the final inversion results from the four contemporaneous sets (sets 1-3, 5 of Table 1). The mode selection criteria were as follows. If a mode was present in one set only it was selected automatically. This was true for most of the modes in the 32-month set. When modes were present in both the BiSON and LOWL sets, the determination with the lower error was selected. When the errors were essentially equal, the average frequency was used, together with the error from just one of the sets, i.e., we took a conservative approach and did not reduce the error when averaging, on the grounds that the errors in the two sets were not independent (there being a correlated contribution due to solar noise). When faced with a choice between the BiSON-8 and BiSON-G data, the BiSON-G data were used if the fit to the BiSON-8 mode was obviously poor. For  $l = 4$  and above, the LOWL data

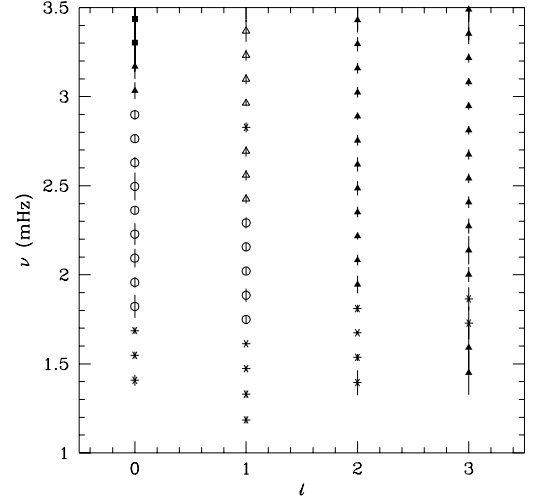


**Figure 5.** The low-degree part of the  $l\text{-}\nu$  diagram of the “best” set. The filled triangles are LOWL modes; circles are BiSON-8 modes; asterisks are modes from the 32-month set; filled squares the BiSON-G modes; and empty triangles averages of LOWL and BiSON-8 modes. The error bars represent  $1000\sigma$  errors.

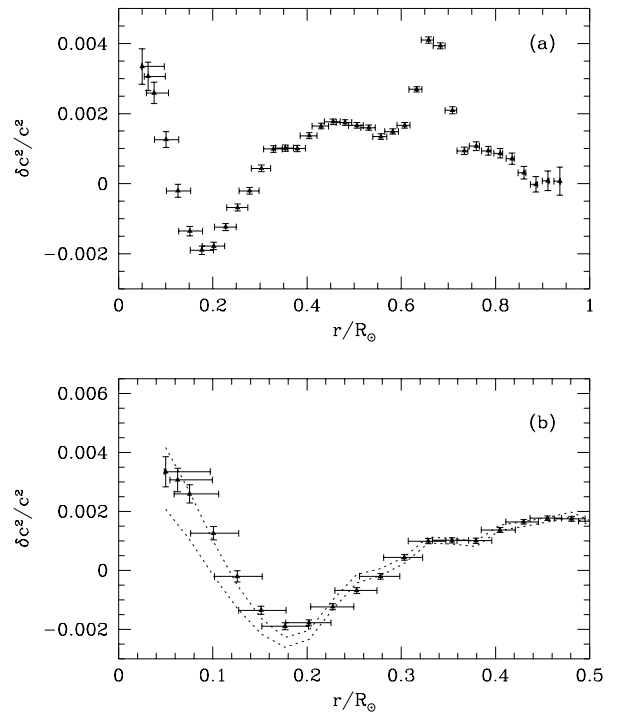


**Figure 6.** The sound-speed inversion results of the “best” set, in the sense (Sun) - (Model). The lower panel (b) concentrates on the results in the core. For comparison, the  $1\sigma$  bounds on the result of inverting just the LOWL set are shown by the dotted line. The plot is on the same scale as Fig. 4.

were used. The  $l \leq 3$  part of the  $l\text{-}\nu$  diagram for the Best Set is shown in Fig. 5.

The sound-speed inversion results of the Best Set are shown in Fig. 6. The main change in the inversion, over the LOWL-only calculation, is that the propagated errors in the core inversion have been reduced substantially, i.e., by more than a factor of two at many radii. The propagated errors in the inversion for the LOWL-only set and Best Set

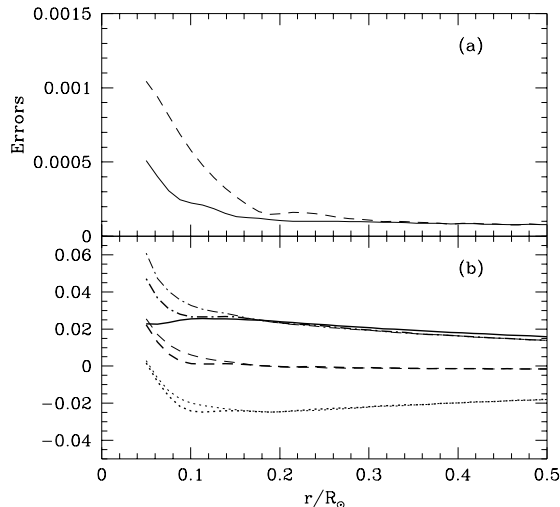


**Figure 7.** A comparison of the propagated errors and resolution of the inversion results of the LOWL and “best” mode sets. The upper panel shows the  $1\sigma$  errors on the solution at different target radii. The dashed line is the error on the inversion results for the LOWL set, while the continuous line is that for the “best” set. In the lower panel, the thick continuous line is the width (in units of the solar radius  $R_\odot$ ) of the averaging kernels for the best set. The thick dotted, thick dashed and thick dot-dashed line are the differences between the first, second and third quartile points and the target radius for the best-set inversion results, all in units of  $R_\odot$ . The thin line shows the corresponding quantities for the inversion with the LOWL data. The width of the averaging kernel, defined as the distance between the first and third quartile points. Note that the averaging kernels become symmetric at around  $0.1R_\odot$ .

are compared in Fig. 7. Note that the influence of the low-degree modes on the errors is restricted to radii less than  $0.35 R_\odot$ . A few averaging kernels have been shown in Fig. 8.

As can be seen from Fig. 7, the data combination also results in a slight improvement in resolution. This can be clearly seen by inverting the frequency differences between the reference and the test model – using only the available modes in each set and weighting by the observed errors. The results of the inversions with the Best Set and LOWL-only set are shown in Fig. 9. The sound-speed difference between the two models increases towards the core. The inverted difference is an average of the exact difference over a finite radius – consequently, unless the averaging is performed over a narrow region, the inverted difference cannot match the exact difference. Thus a higher-resolution inversion will give a better match to the exact differences. While the results are, as expected, identical in the outer layers, the inversion results in the core are not. The results of the Best Set are marginally closer to the exact model differences than are those of the LOWL set alone.

We have also carried out inversions to determine the relative density difference between the Sun and the reference model, using the pair of variables  $(\rho, Y)$ . The results, using both the LOWL-only set and Best Set, are shown in Fig. 10. Unlike the sound-speed inversion results, we find that the density results for the two data sets differ at all radii, even though the sets differ only in low-degree modes which predominantly carry information about the core. Also, the differences in  $\delta\rho/\rho$  are substantially larger than the estimated random errors in the results. Probably the explana-

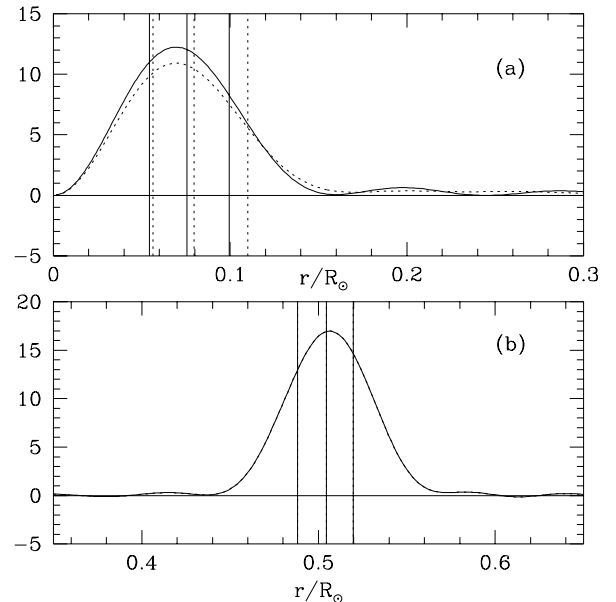


**Figure 8.** The averaging kernels at target radii of (a)  $0.063 R_\odot$  and (b)  $0.51 R_\odot$ . The continuous lines indicate the best-set inversion and the dotted lines the LOWL inversion. Marked on the averaging kernels are the three quartile points. The asymmetry between the positions of the quartile points indicated that the averaging kernels have some structure away from the target radius.

tion for these properties is that our  $(\rho, Y)$  inversion is sensitive to discrepancies between the reference model’s equation of state, which was used in deriving the  $(\rho, Y)$  kernels, and the true equation of state of the solar plasma (cf. Basu & Christensen-Dalsgaard 1997). Note that in this context these discrepancies can also include the effect on  $\Gamma_1$  of differences in the abundance of heavy elements. In additional tests with artificial data we have found comparable effects of using the two different mode sets if the test model was based on the so-called MHD equation of state (e.g. Mihalas, Däppen & Hummer 1988) while the reference model used the OPAL equation of state. It seems credible that the intrinsic error in the OPAL equation of state, relative to the Sun, is of a magnitude similar to the difference between OPAL and MHD. We also note that the mass-conservation constraint,

$$\int \rho \frac{\delta\rho}{\rho} r^2 dr = 0, \quad (5)$$

implies a strong correlation between the results of density inversions at all radii. Thus even if the change in mode set has its primary effect in the core, the inferred density difference is likely to change at all radii, as observed. Such sensitivity to the equation of state can be greatly reduced by using  $(\rho, \Gamma_1)$  or by explicitly seeking to suppress in the  $(\rho, Y)$  inversion any contributions from intrinsic differences in  $\Gamma_1$  (Basu & Christensen-Dalsgaard 1997), although this results in larger random errors in the solution for reasons we have already discussed in Section 1.

As in the case of the sound-speed inversion, the errors in the density inversion are reduced and the resolution improved by using the Best Set, compared with inversion of the LOWL-only set. Also, the tests on artificial data suggest that the effects of errors in the equation of state are

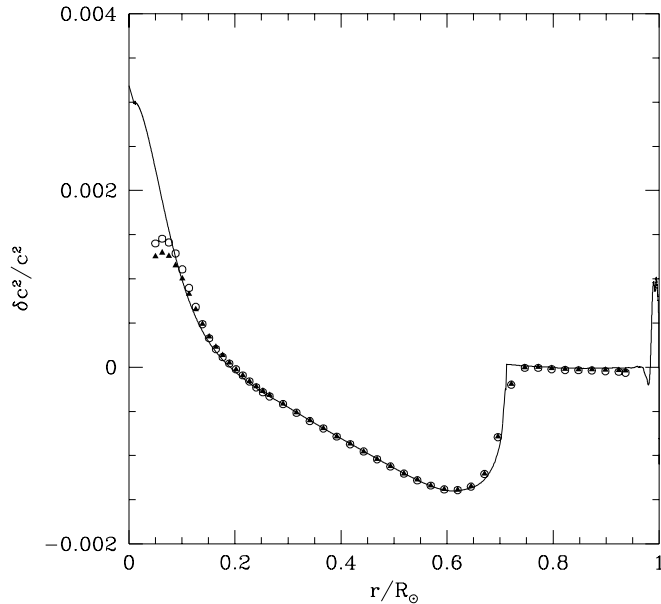


**Figure 9.** The continuous line shows the exact sound-speed difference between the test (4.52 Gyr) and reference (4.6 Gyr) models, in the sense (younger) minus (older). The symbols show the results of the inversion to determine the difference between models. The circles are inversion results using the Best Set modes and the triangles those using the LOWL modes. Note that near the core, the results using the Best Set are closer to the exact difference. This indicates better resolution.

less severe for the Best Set than for LOWL set, probably as a result of the stronger constraints on the core provided by the former set.

## 5 DISCUSSION AND CONCLUSIONS

We have shown that solar-oscillation data from different sources can be successfully combined if the observations are contemporaneous. Although a homogeneous dataset is preferable, different instruments are best suited to observing different ranges of modes. In particular, observations made in integrated sunlight – which are sensitive only to modes of the lowest degrees – can be combined with resolved observations to give a reasonably large selection of modes.

Using contemporaneous data means that corrections for solar cycle effects – which are still very uncertain – are not required. The results obtained from such a combined set are consequently more reliable. The combination of data from the LOWL instrument and the BiSON network shows that the inversion errors in the core can be reduced by a up to a factor of two in the part of the Sun whose structure is the most difficult to determine. The resolution of the inversions is also improved to a certain extent.

We find from Fig. 6 that the sound speed  $c$  of a solar model constructed with the most up-to-date physics available is very close to that of the Sun. The difference in  $c^2$  is at most 0.5 per cent and is considerably less in most regions. However, this small discrepancy is quite substantial compared with the errors in the inversion, as inferred by propagating the data errors. The sound-speed difference

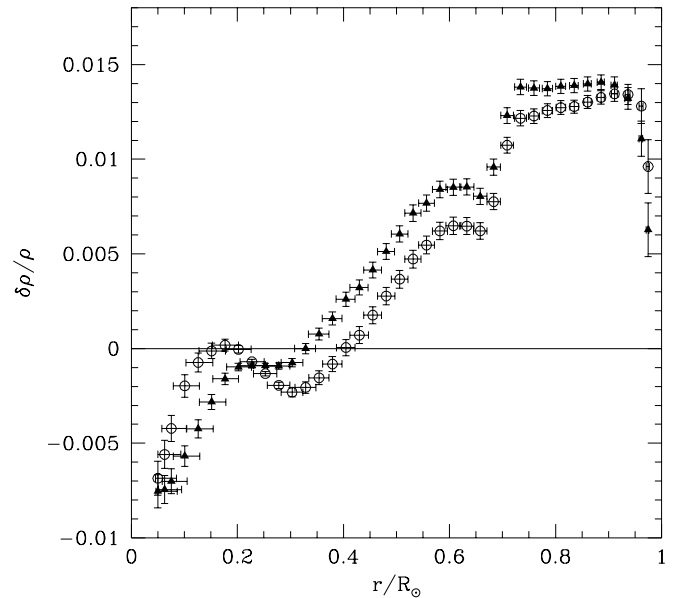


**Figure 10.** The relative density difference between the Sun and the reference model, in the sense (Sun) – (Model), as inferred by the inversion of the LOWL (triangles) and the “best” sets (circles).

between the Sun and the model has three very noticeable features — a large positive bump at roughly  $0.7R_\odot$ , a dip around  $0.2R_\odot$  and a rise in the core. The first feature is just beneath the base of the solar convection zone, which lies at roughly  $0.7R_\odot$  (Christensen-Dalsgaard, Gough & Thompson 1991; Basu & Antia 1997). The sound speed is given by  $c^2 = \Gamma_1 p/\rho \propto \Gamma_1 T/\mu$  in the excellent approximation of an ideal gas. Thus the presence of the first feature could be explained by helium settling being too strong in the model in this region. The increase in the helium abundance increases the mean molecular weight of the material at the convection-zone base, and hence decreases the sound speed in the model. If the gravitational settling has been overestimated, the reason could be that in the Sun the settling is inhibited by some mixing in this region (Gough et al. 1996), a speculation supported by secondary inversions for the helium profile in the Sun (Antia & Chitre 1997). A mismatch in the depth of the convection zones in the model and Sun (Basu & Antia 1997) could also contribute to the feature.

Probing the structure of the energy-generating core provides a particularly important observational test of the theory of stellar evolution. The negative region and the subsequent rise in the sound-speed difference implies that the variation of the sound speed in this region of the Sun is flatter than in the reference model. In this region the abundance varies with position not only because of settling but also due to the burning of hydrogen into helium over the Sun’s lifetime. The inversion results could be explained if some mixing has transported helium outward from the inner core, leading to the Sun’s sound speed being increased in the inner core and decreased around  $0.2R_\odot$ , relative to the model (cf. Gough et al. 1996).

The density differences between the Sun and the reference model, illustrated in Fig. 10, are also of modest size,



although substantial compared with the estimated errors. Overall, the density in the Sun is higher than that in the model, except in the core – the Sun is therefore less centrally condensed than the model. The density difference shows a jump at the base of the convection zone, corresponding to the sharp feature in the sound-speed difference at this location. Density differences within the convection zone are more sensitive to model parameters than the sound speed. Such discrepancies could be caused by differences in convection zone depths and elemental abundances. The results for density show a considerable, and somewhat worrying, sensitivity to the choice of mode set. We have argued that might plausibly be caused by errors in the equation of state assumed in the calculation of the reference model. Such effects can in fact be suppressed in the inversion, although at the expense of a substantial increase in the random errors (cf. Basu & Christensen-Dalsgaard 1997). On a more positive note, the sensitivity hints at the potential to extract even quite subtle information about the equation of state from helioseismic inversions.

The positive sound-speed difference in the core and the smaller central condensation might indicate that the Sun is younger than the assumed age of 4.6 Gyr. Indeed, estimates based on meteoritic ages (e.g. Guenther 1989; Wasserburg, in Bahcall & Pinsonneault 1995) indicate that the age is close to 4.52 Gyr, as assumed in the test model. Comparison of the exact difference in Fig. 9 with the inversion in Fig. 6 shows that using a younger reference model would tend to reduce the difference between the Sun and the model very near the centre, but it would increase it elsewhere. Similarly, Basu et al. (1996a) found that although the density difference between the Sun and a younger model is lower in the core, the differences elsewhere increase. Alternatively, some degree of mixing in the core could resolve both the problem of the larger sound speed and the lower density in the solar core.

## ACKNOWLEDGMENTS

This work was supported in part by the Danish National Research Foundation through its establishment of the Theoretical Astrophysics Center and by the US National Science Foundation through base funding of HAO/NCAR. We would like to thank all those who are – or have been – associated with the BiSON global network and all our hosts at the network sites. BiSON is funded by the UK Particle Physics and Astronomy Research Council.

## REFERENCES

Anderson E. R., Duvall T. L., Jefferies S. M., 1990, *ApJ*, 364, 699  
 Antia H. M., Basu S., 1994, *A&AS*, 107, 421  
 Antia H. M., Chitre S. M., 1997, *ApJ*, submitted  
 Bahcall J. N., Pinsonneault M. H., 1995, *Rev. Mod. Phys.*, 67, 781  
 Balmforth N. J., 1992, *MNRAS*, 255, 639  
 Basu S., Antia H. M., 1997, *MNRAS*, in the press  
 Basu S. Christensen-Dalsgaard J., 1997, *A&A*, submitted  
 Basu S., Christensen-Dalsgaard J., Schou J., Thompson M. J., Tomczyk S., 1995, in Hoeksema J. T., Domingo V., Fleck B., Battrick B., eds, *Proc. Fourth SOHO Workshop: Helioseismology*, Volume 2. ESTEC, Noordwijk, p. 25

Basu S., Christensen-Dalsgaard J., Schou J., Thompson M. J., Tomczyk S. 1996a, *ApJ*, 460, 1064  
 Basu S., Christensen-Dalsgaard J., Schou J., Thompson M. J., Tomczyk S. 1996b, *Bull. Astron. Soc. India*, 24, 147  
 Basu S., Christensen-Dalsgaard J., Pérez Hernández, F., Thompson M. J., 1996c, *MNRAS*, 280, 651  
 Chandrasekhar S., 1964, *ApJ*, 139, 664  
 Chaplin W. J., Elsworth Y., Howe R., Isaak G. R., McLeod C. P., Miller B. A., van der Raay H. B., Wheeler S. J., New R., 1996a, *Sol. Phys.*, 168, 1  
 Chaplin W. J., Elsworth Y., Howe R., Isaak G. R., McLeod C. P., Miller B. A., New R., 1996b, *MNRAS*, 282, L15  
 Christensen-Dalsgaard J., 1986, in Gough D. O., ed, *Seismology of the Sun and the distant Stars*. Reidel, Dordrecht, p. 23.  
 Christensen-Dalsgaard J., Berthomieu G., 1991, in Cox A. N., Livingston W. C., Matthews M., eds, *Solar Interior and Atmosphere*. University of Arizona Press, Tucson, p. 401  
 Christensen-Dalsgaard J., Gough D. O. Pérez Hernández F., 1988, *MNRAS*, 235, 875  
 Christensen-Dalsgaard J., Gough D. O., Thompson M. J., 1991, *ApJ*, 378, 413  
 Christensen-Dalsgaard J., Däppen W., Ajukov S. V., et al., 1996, *Science*, 272, 1286  
 Cox A. N., Kidman R. B., 1984, in *Theoretical problems in stellar stability and oscillations*. Institut d’Astrophysique, Liège, p. 259  
 Däppen W., Gough D. O., Kosovichev A. G., Thompson M. J., 1991, in Gough D. O., Toomre J., eds, *Lecture Notes in Physics*, 388. Springer, Heidelberg, p. 111  
 Dziembowski W. A., Pamyatnykh A. A., Sienkiewicz R., 1990, *MNRAS*, 244, 542  
 Dziembowski W. A., Pamyatnykh A. A., Sienkiewicz R., 1991, *MNRAS*, 249, 602  
 Dziembowski W. A., Goode P. R., Pamyatnykh A. A., Sienkiewicz R., 1994, *ApJ*, 432, 417  
 Elsworth Y., Howe R., Isaak G. R., McLeod C. P., Miller B. A., New R., Speake C. C., Wheeler S. J., 1994, *ApJ*, 434, 801  
 Gough D. O., 1990, in Osaki Y., Shibahashi H., eds, *Lecture Notes in Physics*, 367. Springer, Berlin, p. 283  
 Gough D. O., Kosovichev A. G., 1993, *MNRAS*, 264, 522  
 Gough D. O., Kosovichev A. G., Toutain T., 1995, *Solar Phys.*, 157, 1  
 Gough D. O., Kosovichev A. G., Toomre J., et al., 1996, *Science*, 272, 1296  
 Grevesse, N., Noels, A. 1993, in Prantzos N., Vangioni-Flam E., Cassé M., eds, *Origin and evolution of the Elements*. Cambridge Univ. Press, Cambridge, p. 15  
 Guenther D. B., 1989, *ApJ*, 339, 1156  
 Iglesias C. A., Rogers F. J., Wilson B. G., 1992, *ApJ*, 397, 717  
 Kosovichev A. G., Christensen-Dalsgaard J., Däppen, W., Dziembowski W. A., Gough D. O., Thompson M. J., 1992, *MNRAS*, 259, 536  
 Kurucz R. L., 1991, in Crivelli L., Hubeny I., Hummer D. G., eds, *Stellar atmospheres: beyond classical models*. NATO ASI Series, Kluwer, Dordrecht, p. 441  
 Libbrecht K. G., Woodard M. F., 1990, *Nature*, 345, 779  
 Mihalas D., Däppen W., Hummer D. G., 1988, *ApJ*, 331, 815  
 Pijpers F. P., Thompson M. J., 1992, *A&A*, 262, L33  
 Rogers F. J., Swenson F. J., Iglesias C. A., 1996, *ApJ*, 456, 902  
 Schou J., 1992. Ph.D thesis, Aarhus University.  
 Tomczyk S., Streander K., Card G., Elmore D., Hull H., Cacciani A., 1995, *Sol. Phys.*, 159, 1  
 Toutain T., Appourchaux T., 1994, *A&A*, 289, 649  
 Unno W., Osaki Y., Shibahashi H., 1989, *Non-radial Oscillations of Stars*, 2nd ed.. Univ. of Tokyo Press, Tokyo

This paper has been produced using the Royal Astronomical Society/Blackwell Science  $\text{\TeX}$  macros.